A scanning apertureless fluorescence microscope

Guillaume A. Lessard, T. J. Yang, Pierre Barritault, Stephen R. Quake

Department of Applied Physics, California Institute of Technology, Pasadena, USA

ABSTRACT

We describe a near-field apertureless fluorescence microscope, capable of imaging fluorescent latex beads with sub-wavelength precision. The instrument is based on a home-built tapping-mode atomic-force microscope (AFM), to which an inverted optical microscope was added. The fact that the wavelength of the fluorescence that we observe is different from the wavelength of the illumination allows for a relatively straightforward detection mechanism. Sample images are presented, along with evidence that the observed effect is of optical origin.

Keywords: Near-field, optics, AFM, fluorescence, force, light, apertureless NSOM

1. INTRODUCTION

In the last fifteen years, the development of the near-field scanning optical microscope (NSOM) has generated a lot of activity.[1–3] The usual NSOM involves the transmission of light to and/or from the tapered end of a metal-coated optical fiber. Tapered coated fiber probes have a resolving power of 30-50 nm,[4] but cannot resolve much more than that, in addition to being susceptible to artifacts.[4,5]

As a response to this limitation, apertureless near-field microscopy was proposed.[6,7] In this scheme, a sharp probe periodically perturbs the interaction between a sample and its illumination. The perturbation can involve probe-induced phase shifts in the reflected electric fields,[8] or it can involve the periodic occlusion of the illuminating beam by the sharp probe.[9] In all cases, measurement of this perturbation involves lock-in detection. The perturbation is synchronous with the probe movement: the interaction of the sample with the probe is not the same at the low point than at the high point of the probe trajectory. Lock-in detection thus allows the discrimination of the near-field information (which is modulated at the probe's oscillation frequency) from the far-field optical information (which varies more slowly).

By using fluorescence for apertureless NSOM, we can sidestep many artifacts that are a risk for other, single-wavelength NSOM techniques. With a relatively clean system, we can be certain that the sole source of fluorescence in the system is the sample itself. Also, fluorescence being an optical phenomenon, we can analyze its behavior and further control the presence of non-optical artifacts.

We present here a new apertureless fluorescence microscope. We believe these are the first reported images of fluorescence by apertureless NSOM techniques. We first describe the experimental setup, and results are presented. We then demonstrate that the imaging relies on a truly optical contrast mechanism.

2. EXPERIMENTAL SETUP

The experimental setup is shown in figures 1 and 2. The part of the setup that examines the sample is described in figure 1, while the signal pathways are described in figure 2. The sample is scanned simultaneously by a tapping-mode AFM and by a focused laser beam. The laser is a green-emitting HeNe (model 1674P from Uniphase), with a wavelength of 543.5 nm. The probe oscillates with an amplitude of 75 to 100 nm; when the probe is at the bottom of its trajectory, it affects the interaction of the green photons with the sample, while it doesn't affect the fluorescence when at the top of its trajectory. The AFM cantilever's resonance frequency lies between 250 and 300 kHz, allowing the use of lock-in detection. We excite the AFM at a frequency f_0 slightly below the resonance frequency of the cantilever, for stability reasons. The AFM probe is positioned at the center of the diffraction-limited laser spot, in order to produce the greatest possible perturbation of the laser-sample interaction.

The red fluorescence photons are detected using with an EG&G SPCM AQ-131 photon detector, placed behind an optical long-pass filter. The output of the photon detector is fed simultaneously to two systems: an event counter

Correspondence (to S. R. Q.): e-mail: quake@its.caltech.edu; WWW: http://thebigone.caltech.edu/quake/

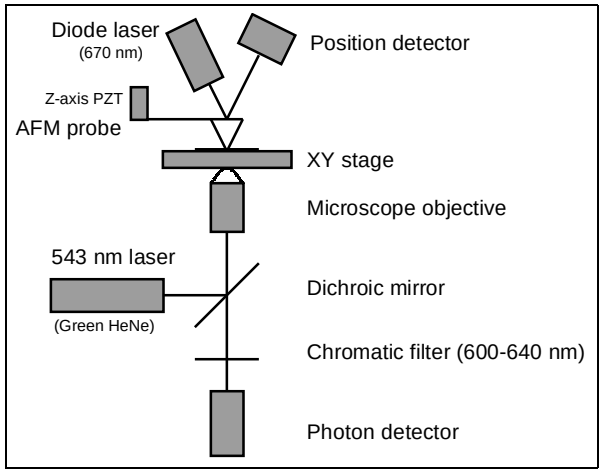

Figure 1. Experimental setup, optics and AFM

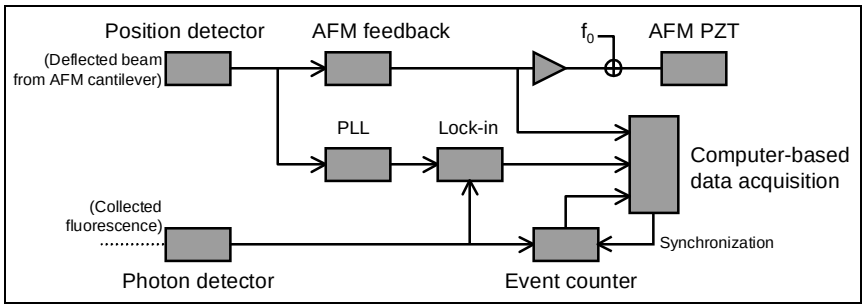

Figure 2. Experimental setup, electrical signals and control

and a lock-in amplifier. The event counter is used to obtain a total photon count per pixel in order to obtain a far-field image, while the lock-in amplifier allows us to detect the near-field effect.

The reference input of the lock-in is a sine wave that is in phase with the movement of the AFM probe. The output of the AFM's position detector is fed into a PLL, the output of which acts as the lock-in's reference input. This ensures that the reference to the lock-in is stable in amplitude, and information about the AFM probe's behavior is not electrically coupled into the measured optical signal. The bandwidth of our lock-in amplifier's output filter was chosen to be 60 Hz, as a compromise between scanning speed and noise rejection.

The signal of interest for our imaging is the output of the lock-in amplifier. This will be proportional to the perturbation that is induced by the probe when it is at the low point of its trajectory. The length scale of this interaction should be dependent on tip size, as has been reported for other apertureless NSOM techniques.[8,10,11]

The AFM used in this experiment is a home-built, tapping-mode AFM. A feedback loop utilizing the oscillation amplitude of the probe controls the AFM. The goal of this AFM was not high resolution, so its resolution is stage-limited at roughly 4 nm for the moment. The probes that were used are etched silicon probes by Nanosensors.

The inverted optical microscope is composed of an infinity-corrected 60X objective with a numerical aperture of 1.4 (Olympus PlanApo 60X/1.40 Oil infinity/0.17), plus a 250 mm lens focusing the fluorescent beam onto the photon detector's active area. The diameter of the laser spot is between 350 and 450 nm.

3. RESULTS

3.1. Images

To obtain images, the AFM probe and the focused laser beam are held still in the XY plane while the sample is scanned. In addition to collecting the output signal from the lock-in amplifier, we collect the Z-feedback (topography)

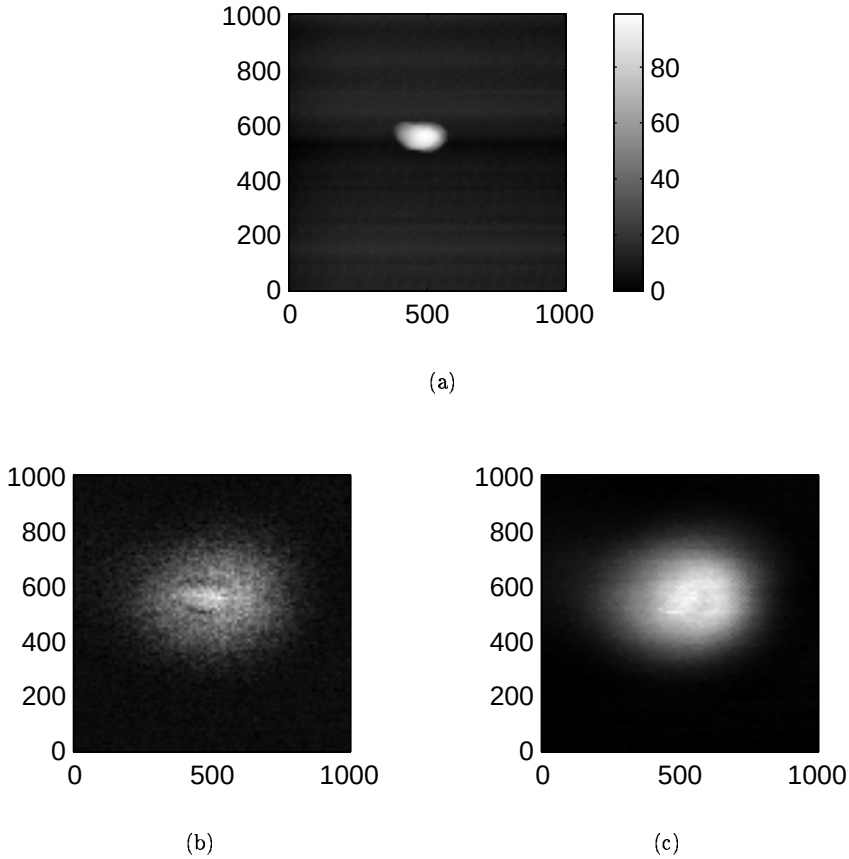

Figure 3. Images of a fluorescent 100 nm bead. All scales are in nanometers (a) AFM image (vertical scale in nanometers), (b) near-field image, (c) far-field image.

signal from the AFM as well as the total photon count per pixel. This way, we obtain three images: topographical, far-field optical and near-field optical.

The near-field optical image, being the output of a lock-in amplifier, is for all practical purposes a 120 Hz-wide section of the photon detector output's power spectrum, centered at f_0 (the tapping frequency of the AFM probe). The output of the photon detector is a 10 ns pulse for each photon detected. This narrow pulse has a wide spectrum, including components at and around f_0. When taking an image, we typically get total photon counts of 10^5 photons per second, with maxima of 5×10^5 to 10^6 photons per second. This means that, at f_0, there is always a background noise, proportional to the far-field intensity. The tip-induced fluorescence enhancement is, in our experience, between 5 and 20 dB above the level of the background noise, This means that our near-field images are a superposition of the background noise (similar to the far-field image) and of the field-enhanced image. A future refinement of the lock-in amplifier will deal with removing this background.

The sample used for these images is composed of fluorescent latex beads (Interfacial Dynamics Corporation), 100 nm in diameter, spread onto a clean cover glass. The fluorescent dye incorporated in the beads is Nile Red. The absorption peak of Nile Red is around 520 nm, and its emission peak is around 580 nm. The power of the 543.5 nm laser beam prior to entering the system was 3.3 μW.

Figure 3 shows 1 μm^2 images of a single bead by (a)AFM, (b)near-field and (c)far-field. The image of fig. 3(b) is actually a superposition of the near-field image with the far-field, as outlined earlier.

Figures 4 and 5 show comparisons between the near-field and far-field images, in a 100 nm-wide vertical cross-section of both images, coinciding with the observed bead's position. Figure 4 illustrates that the near-field signal is

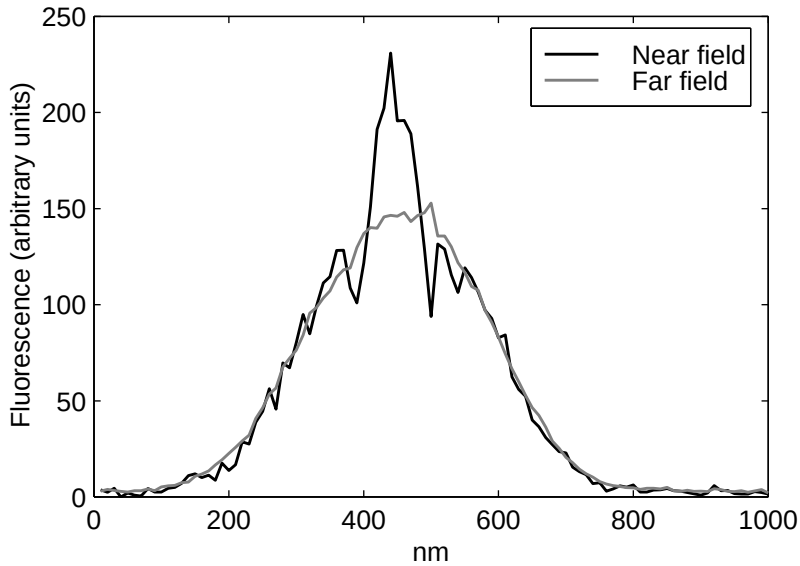

Figure 4. Comparison of the vertical cross-sections of the near-field (fig. 3(a)) and the far-field (fig. 3(b)) images. The two curves follow each other closely until the central 100 nm, the position of the observed bead. Over the bead, the near-field image shows a sharp local enhancement.

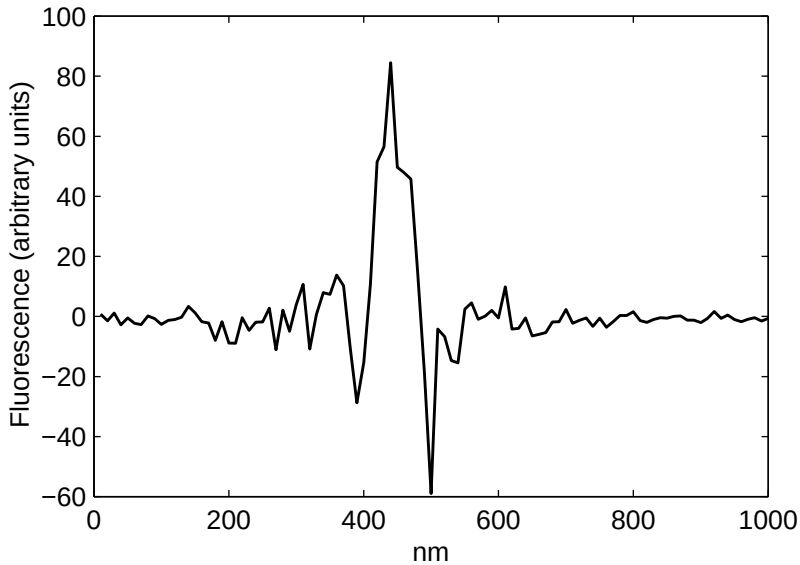

Figure 5. Difference between the two curves shown in fig. 4. The difference between the two signals is small until the central 100 nm, which correspond to the position of the bead.

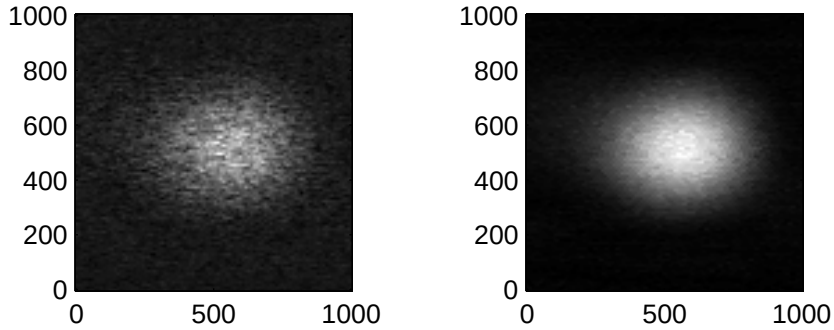

Figure 6. Images of the bead of fig. 3 with the AFM probe pulled away. (a) near-field image, (b) far-field image. The near-field image is the same (allowing for noise) as the far-field image; the enhancement effect is gone.

superimposed on the far-field signal in figure 3(b), and that the near-field resolution of our system is well below the absolute limit of approximately 220 nm that is imposed by diffraction.

3.2. Discussion

In order to verify that the imaging is not the result of an artifact, various manipulations have been made. The simplest is to pull the AFM probe away from the surface, and to take an image. An image obtained this way will have the same far-field component, but the near-field component disappears. The images of figure 6 were obtained immediately after the images from figure 3, with the probe pulled away from the surface. There is no fluorescence enhancement effect.

We have also controlled the images of fig. 3 by blocking the optical excitation in order to verify that it is not a result of a kind of Z-motion artifact. With our final experimental setup, we obtain an image like that from figure 7(a), where there is very little leakage from the Z-motion to the lock-in output. In fact, the noise level shown in this image is much lower than the noise level present when there is a non-negligible optical input. Furthermore, the AFM image of fig. 3(a) does not perfectly superimpose over the "hump" of the near-field image (fig. 3(b)), showing further that it is not a Z-motion artifact.

In order to illustrate the artifacts induced by the use of the wrong reference for the lock-in detector, we include figure 7(b), where the lock-in reference is directly the probe position. There is a large leakage, entirely caused by the AFM feedback circuit's error. As a feedback cannot be without error, this will always happen to some extent. A similar problem would occur if we were to directly utilize the function generator as lock-in reference, as the probe's phase shift with respect to the function generator varies with respect to the conditions of the examined surface.

A more formal verification of the fluorescence enhancement can be made by examining the power spectrum of the photon detector's output signal. When the AFM probe is properly aligned with the focused laser beam, the power spectrum shows a peak (5-20 dB) at the tapping frequency of the probe, as can be seen on figure 8. If there really is enhanced fluorescence in the presence of the probe, the photobleaching should be enhanced locally; if there is such an enhanced photobleaching, the peak will decay faster than the background noise.

Figure 9 shows the evolution of the fluorescence enhancement peak and of the fluorescence background as a function of time. The measurement is made by parking the XY stage and letting data acquisition proceed for a long period of time when a 100 nm bead is under the AFM probe. In this case the laser power was 50 μW in order to acquire the data in reasonably short time and thus reduce the risk of mechanical drift during the period of data acquisition. After the measurement, we verified that the drift had been negligible during the measurement. Each pair of points is from a different power spectrum snapshot.

We can see in fig. 9 that the peak corresponding to synchronized photons decays faster than the level of background fluorescence. We explain this by an enhanced field intensity in presence of the AFM probe. Before being

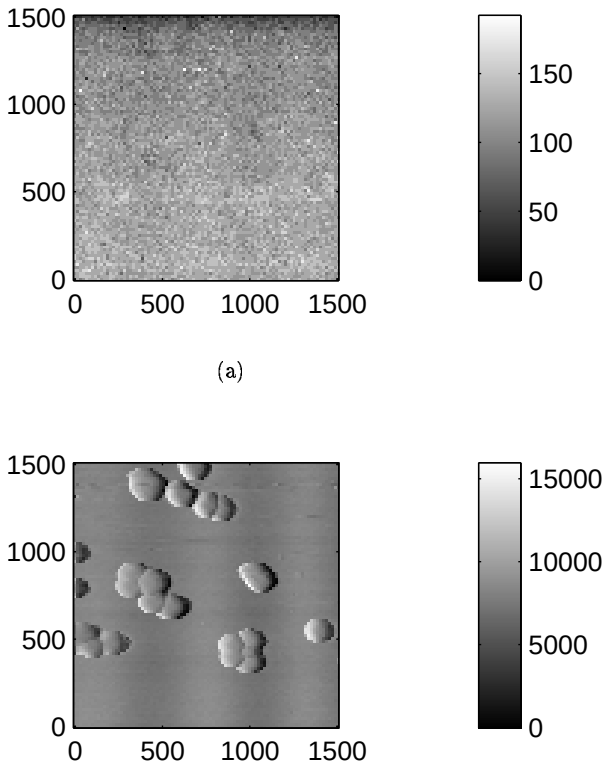

Figure 7. Lock-in output with no optical signal, while the AFM probe is imaging. (a) PLL as lock-in reference, (b) probe position as reference. If the incorrect signal is chosen as lock-in reference, the resulting image can be misleading. Note the scales of images (a) and (b); if (a) were shown at the same scale as (b), it would appear completely black.

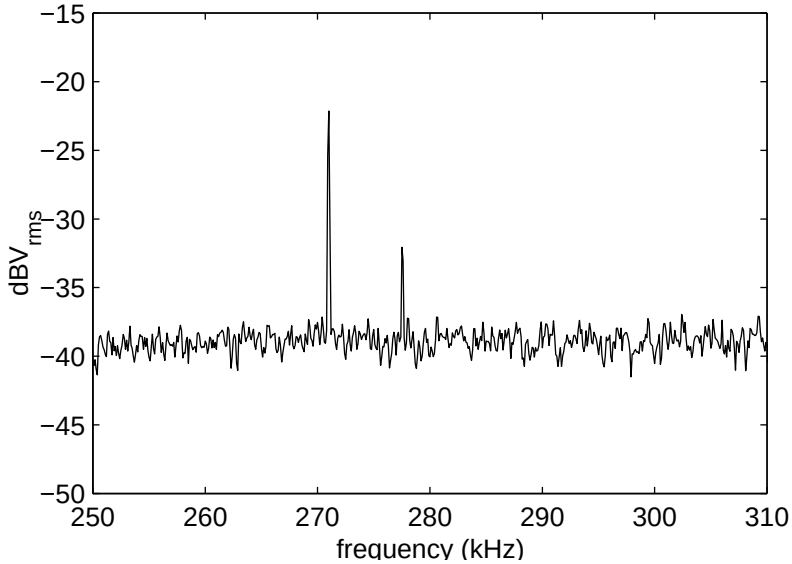

Figure 8. A sample power spectrum of the output from the photon detector. The large peak at 270 kHz is at the probe's resonance frequency. The second peak at 277 kHz is an artifact caused by the AFM feedback circuit; it is also probe-induced.

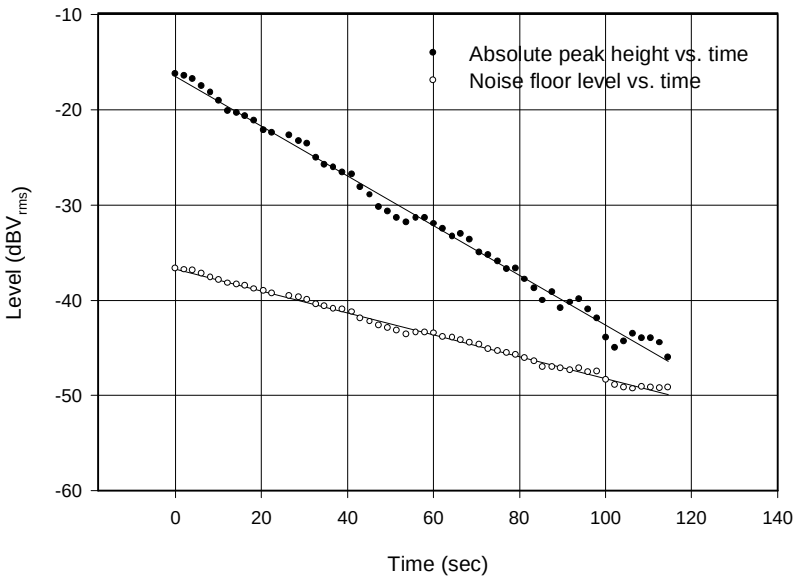

Figure 9. Evolution of the fluorescence enhancement peak and of the background as a function of time, as the probe is held stationary over a fluorescent bead. The peak, representing the photons synchronized with the AFM probe, decays at a greater rate than the background photons. This shows that there is an enhancement of the fluorescence at the probe tip.

photobleached, each fluorescent molecule emits a number of fluorescence photons on the order of 10^6. If the light intensity illuminating a molecule is stronger, those 10^6 photons will be emitted in a shorter period of time, resulting globally in a greater decay rate. In our measurement, we see a greater decay rate for photons synchronized with the AFM probe than for non-synchronized photons, suggesting that there is a probe-induced fluorescence enhancement. We believe that the subwavelength contrast from figure 3 is a result of the same phenomenon.

4. CONCLUSION

We have demonstrated the basic principles of a scanning apertureless fluorescence microscope. The use of fluorescence for apertureless near-field microscopy allows us to use a non-interferometric detection mechanism, based on periodic perturbation of the interaction between a sample and an illumination source. We have shown imaging results demonstrating subwavelength resolution, as well as supporting measurements that show that the effect is probe-related, optical contrast mechanism. Further enhancements include improving the resolution of the apparatus, as well as improving the rejection of the far-field signal from the near-field image. A more sophisticated lock-in detection scheme will allow unambiguous isolation of the probe-enhanced signal from the far-field background.

ACKNOWLEDGMENTS

This work was supported by the Keck Foundation. G. L. had partial financial support from the Fonds FCAR.

REFERENCES

1. D. W. Pohl, W. Denk, and M. Lanz, "Optical stethoscopy - image recording with resolution $\lambda/20$," *Applied Physics Letters* **44**(7), pp. 651–653, 1984.
2. M. Paesler and N. van Hulst, eds., *Ultramicroscopy*, vol. 61 (1-4), (Amsterdam), Elsevier Science, 1995.
3. M. A. Paesler and P. J. Moyer, *Near Field Optics Theory, Instrumentation and Applications*, Wiley, New York, 1996.
4. B. Hecht, H. Bielefeldt, Y. Inouye, D. W. Pohl, and L. Novotvy, "Facts and artifacts in near-field microscopy," *Journal of Applied Physics* **81**(6), pp. 2492–2498, 1997.
5. V. Sandoghdar, S. Wegscheider, G. Krausch, and J. Mlynek, "Reflection scanning near-field optical microscopy with uncoated fiber tips: How good is the resolution really?," *Journal of Applied Physics* **81**(6), pp. 2499–2503, 1997.
6. F. Zenhausern, M. P. O'Boyle, and H. K. Wickramasinghe, "Apertureless near-field optical microscope," *Applied Physics Letters* **65**(13), pp. 1623–1625, 1994.
7. Y. Inouye and S. Kawata, "Near-field scanning optical microscope with a metallic probe tip," *Optics Letters* **19**(3), pp. 159–161, 1994.
8. F. Zenhausern, Y. Martin, and H. K. Wickramasinghe, "Scanning interferometric apertureless microscopy - optical imaging at 10 angstrom resolution," *Science* **269**(5227), pp. 1083–1085, 1995.
9. P. Gleyzes, A. C. Boccara, and R. Bachelot, "Near-field optical microscopy using a metallic vibrating tip," *Ultramicroscopy* **57**(2-3), pp. 318–322, 1995.
10. H. Furukawa and S. Kawata, "Local field enhancement with an apertureless near-field-microscope probe," *Optics Communications* **148**(4-6), pp. 221–224, 1998.
11. A. Lahrech, R. Bachelot, P. Gleyzes, and A. C. Boccara, "Infrared-reflection-mode near-field microscopy using an apertureless probe with a resolution of $\lambda/600$," *Optics letters* **21**(17), pp. 1315–1317, 1996.